Analysis of the efficiency of intermediate band solar cells based on quantum dot supercrystals

S. Heshmati, S. Golmohammadi, K. Abedi, H. Taleb

Abstract. **We have studied the influence of the quantum-dot (QD) width and the quantum-dot conduction band (QD-CB) offset on the efficiency of quantum-dot intermediate band solar cells (QD-IBSCs). Simulation results demonstrate that with increasing QD-CB offset and decreasing QD width, the maximum efficiency is achieved.**

1. Introduction

Quantum-dot intermediate band solar cells (QD-IBSCs) are the newest type of solar cells, which make it possible to attain the maximum efficiency. Realisation of low-cost photovoltaic power sources is subject to development of low cost and efficient solar cells. The performance of intermediate band solar cells (IBSCs) depends on the electrical and optical properties of the intermediate band (IB) material. These properties are characterised by an electronic band that is located between the conduction band (CB) and the valence band (VB) of a conventional semiconductor bandgap. The IBSC has been proposed by using QD technology [1–3].

The structure of quantum dots plays an important role to achieve maximum efficiency. The energy conversion efficiency is a fundamental parameter in photovoltaic solar cell technology [4]. It is defined as

$$\eta = F V_{\mathrm{OC}} J_{\mathrm{SC}} / P_{\mathrm{in}}, \qquad (1)$$

where F is the fill factor; V_{OC} is the open circuit voltage; J_{SC} is the short-circuit current density; and P_{in} is the incident power per unit area [4].

The ideal performance of a solar cell is realised, when the bandgaps separating the intermediate bands (IBs) from the CB and from the VB, lie near 1.24 eV and 0.71 eV, respectively [5, 6] (Fig. 1). These gaps can be located in the opposite way,
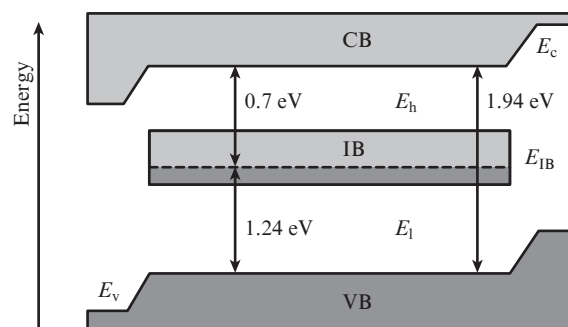
S. Heshmati Department of Engineering, Islamic Azad University, Buin Branch, Iran;
S. Golmohammadi Nanophotonics Group, School of Engineering-Emerging Technologies, University of Tabriz, Tabriz 5166614761, Iran; e-mail: sgolmohammadi@tabrizu.ac.ir;
K. Abedi, H. Taleb Department of Electrical Engineering, Faculty of Electrical and Computer Engineering, Shahid Beheshti University, G. C. 1983963113, Tehran, Iran

Figure 1. IBSCs with an optimal bandgap.

i.e., the IB could be closer to the VB than to the CB. On the other hand, the IB must be partially filled with electrons so that there exist empty states for receiving the electrons pumped from the VB and electrons-filled states to provide for the electrons pumped to the CB [7].

A semiconductor with a single bandgap absorbs only photons with energies above the bandgap threshold, E_{g}. Therefore, only these photons contribute into the produced photocurrent. However, when the IB is half-filled, two photons with energies below the bandgap threshold, E_{g}, can pump an electron from the VB to the CB. The first photon with an energy greater than E_{l} will pump an electron from the VB to the IB that has empty states for receiving the electron and the other photon with an energy greater than E_{h} will pump an electron from the IB having electron-filled states to the CB [8]. In this method, photocurrent is greater than the current that can be produced by semiconductors with a single bandgap [5–7]. In the radiative limit, the IBSC shows a limiting efficiency of 63.2 % [5, 6], which is significantly higher than the single gap solar cell efficiency (40.7 %) and two-junction solar cell efficiency (55.4 %), operating in the radiative limit. However, in this paper we study the relationship between such QD parameters as CB offset, QD width and QD barrier width in order to achieve the maximum efficiency.

2. Analysis of a single QD and coupled QDs and their relationship with the IB

In order to study the efficiency of QD-IBSCs, two cases are investigated:

(i) QDs are used as individual objects and are not coupled with other dots;

(ii) QDs are coupled with other dots so that the overlap between the QD wave functions forms a miniband which acts as a proper intermediate band [3].
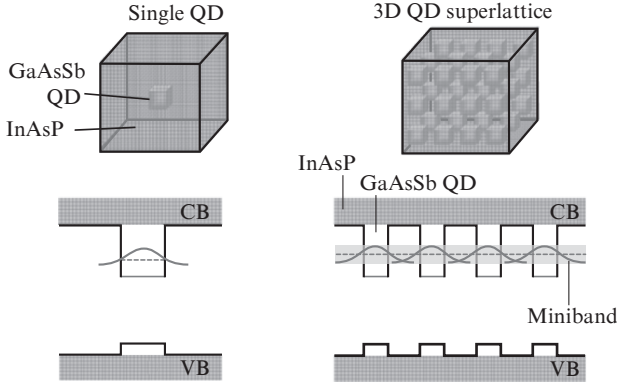
Figure 2. Single and coupled QDs.

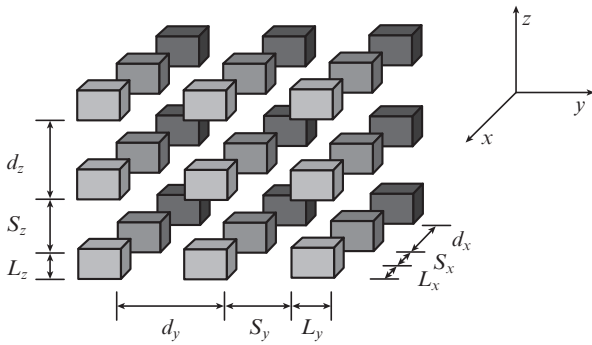The wave functions of a single QD and an ensemble of coupled QDs are shown in Fig. 3.

Figure 3. QD superlattice [10] with a regularly spaced array of equally sized cubic dots in a dielectric matrix.

In our simulations use is made of the barrier/QD material, $GaAs_{0.98}Sb_{0.02}/InAs_{0.49}P_{0.51}$, with an AlAs substrate. The bandgap of the barrier material is 1.48 eV and that of the QD is 0.91 eV. The effective mass of the electron in the barrier material is $0.066m_0$ and in the QD is $0.039m_0$ (m_0 is the electron rest mass). In this material system the energy difference between the conduction band energies of $GaAs_{0.98}Sb_{0.02}$ and $InAs_{0.49}P_{0.51}$ is ~0.57 eV [9].

Calculation of the QD conduction band energy using an effective mass approach. The conduction band energy of an idealised version of a three-dimensional silicon QD superlattice with a regularly spaced array of equally sized cubic dots in a dielectric matrix (Fig. 3) can be calculated using an effective mass approach [10]. In this approach the motion of a carrier in the material system is defined by the effective mass equation [10]

$$\frac{\hbar^2}{2}\nabla\left[\frac{1}{m^*(r)}\nabla\varphi(r)\right]+[E-V(r)]\varphi(r)=0, \qquad (2)$$

where $m^*(r)$ is the effective mass tensor; E is the total energy; $\varphi(r)$ is the envelope of the electron wave function; and $V(r)$ is the microscopic potential seen by the electron, which is considered the sum of three independent periodic functions:

$$V(r) = V_x(r) + V_y(r) + V_z(r). \qquad (3)$$

Consequently, for the case of isotropic effective mass the three-dimensional effective mass equation is separable and reduced to three one-dimensional quantum-well superlattice equations [11]. As a result, the solution to Eqn (2) can be expressed in terms of solutions of the simple one-dimensional Kronig–Penny model [11]. In the case of the isotropic effective mass the corresponding equations are defined as

$$\cos(q_i d_i) = \cos(k_i^D L_i)\cos(k_i^B S_i) - \frac{1}{2}$$

$$\times\left(\frac{k_i^B m_{Di}^*}{k_i^D m_{Bi}^*} + \frac{k_i^D m_{Bi}^*}{k_i^B m_{Di}^*}\right)\sin(k_i^D L_i)\sin(k_i^B S_i), \text{ if } E_i \geqslant V_0, \qquad (4)$$

$$\cos(q_i d_i) = \cos(k_i^D L_i)\cosh(k_i^B S_i) - \frac{1}{2}$$

$$\times\left(\frac{k_i^B m_{Di}^*}{k_i^D m_{Bi}^*} + \frac{k_i^D m_{Bi}^*}{k_i^B m_{Di}^*}\right)\sin(k_i^D L_i)\sinh(k_i^B S_i), \text{ if } 0 < E_i < V_0. \qquad (5)$$
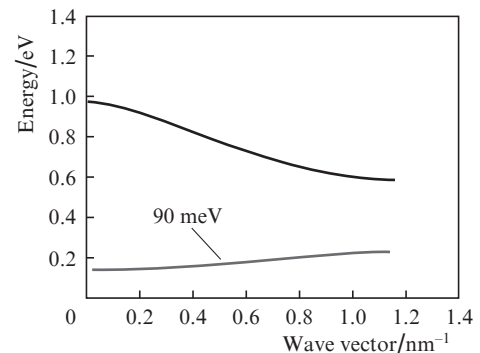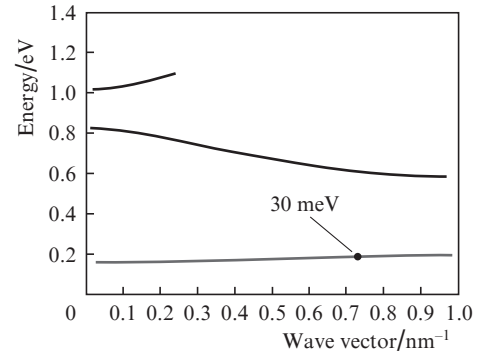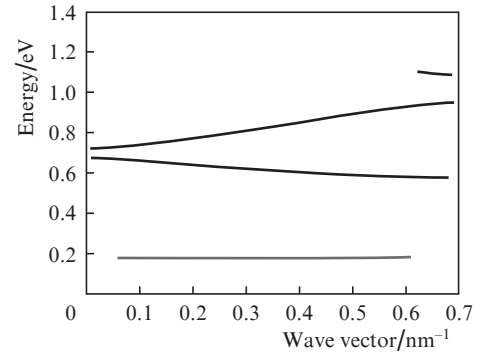

Figure 4. Energy dispersion diagram vs. electron wave functions at (a) a barrier width of 6 nm and IB width of 0 eV, (b) barrier width of 3 nm and IB width of 30 meV and (c) barrier width of 2 nm and IB width of 90 meV. In all the cases the QD width is 4 nm.

In Eqns (4) and (5) $k_i^B = \sqrt{2m_{Bi}^* |E_i - V_0|}/\hbar$; m_{Bi}^* is the effective mass in the dielectric matrix; $k_i^D = \sqrt{2m_{Di}^* |E_i|}/\hbar$; m_{Di}^* is the effective mass of the QD; V_0 is the bias voltage; q_i is the wave vector component; and i is the coordinate x, y, z [11]. The energy dispersion relation is then obtained from

$$E(q) = E_x(q) + E_y(q) + E_z(q). \tag{6}$$

Using the Kronig–Penny model [11, 12] we have obtained the energy dispersion diagrams – dependences of energy on the electron wave vector (Fig. 4) – for three values of the barrier widths at a fixed width of the QD (4 nm).

In this case, the IB is characterised by the first band (electron wave function). There is no overlap between the QD wave functions and, therefore, no broadening in the IB (Fig. 4a). The smallest distance between the QDs leads to the fact that the energy bands or electron wave functions become coupled with each other and a miniband is formed (Figs 4b and c).

The width of the IB or miniband decreases with increasing barrier width (Fig. 5).
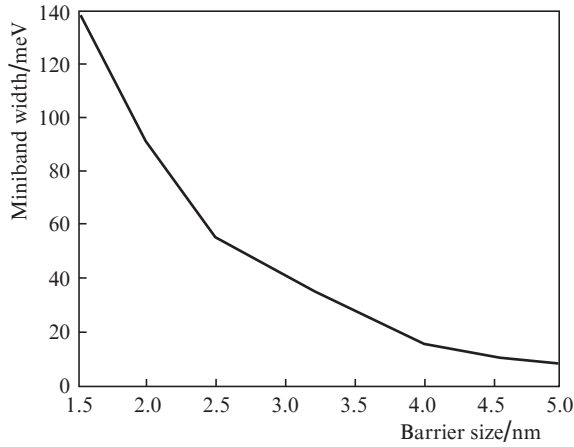
Figure 5. Dependence of the IB (miniband) width on the barrier layer size.

3. Relationship between the QD-CB offset and the QD width

To achieve the maximum efficiency, we investigate in this section the relationship between the QD-CB offset and the width of the QDs.

Design rules for a QD-IBSC. Design rules for selecting the QD-IBSC material triad (QD/barrier/substrate) are as follows [5, 9, 13]:

– the barrier material must have a bandgap in the range from 1.43 eV to 2.56 eV;

– the valence band offset must be negligibly small;

– the material with a direct bandgap must be used because it has a larger absorption coefficient;

– the offset between the CB edges (E_{CB}) must be greater than $0.48E_{CB} - 0.22$;

– the average distance between self-assembled QDs should be such that the overlap between the IB, CB and VB is prohibited.

Examination of different materials with different bandgaps. In the following, we study three different materials in the design of the QD-IBSCs: InAsP/GaAsSb/AlAs, GaInAs/GaAsSb/AlAs and AlInAs/AlGaAs/AlAs.

In InAsP/GaAsSb/AlAs, $GaAs_xSb_{1-x}$ with the mole fraction $x = 0.98$ is used as the barrier material. The value of the bandgap at this specific mole fraction of this material is 1.48 eV [11]. The QD material is $InAs_{1-x}P_x$ with different mole fractions. The value of the bandgap of the QD material is [14]

$$E_g = 0.36 + 0.891x + 0.101x^2. \tag{7}$$

The dependence of the bandgap and the QD-CB offset on the mole fraction is shown in Fig. 6.
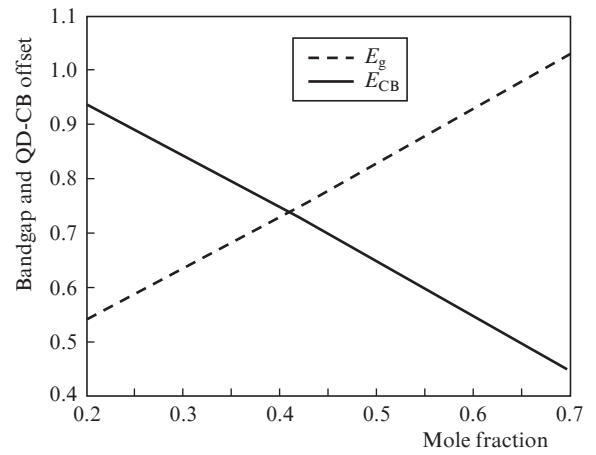
Figure 6. Bandgap and QD-CB offset vs. mole fraction x for InAsP/GaAsSb/AlAs.

The calculated efficiencies at different mole fractions, QD-CB offsets, QD widths and barrier widths are shown in Table 1.

Table 1. Efficiency at different QD parameters for InAsP/GaAsSb/AlAs.

Mole fraction	CB offset/eV	QD width/nm	Barrier width/nm	Efficiency (%)
0.45	0.7	3.8	2	51.50
0.45	0.7	3.8	2.5	52.34
0.5	0.65	3.9	2	50.99
0.5	0.65	3.9	2.5	51.73
0.55	0.6	3.9	2	49.97
0.55	0.6	3.9	2.5	50.58
0.6	0.55	4	2.5	49.47
0.7	0.45	4.2	2.5	46.51

One can see that with increasing mole fraction, the efficiency and the CB offset decrease. Therefore, the maximum efficiency is achieved for the QD and barrier material widths of 3.8 and 2.5 nm, respectively.

In GaInAs/GaAsSb/AlAs, $GaAs_xSb_{1-x}$ also has the mole fraction $x = 0.98$ and the value of the bandgap at this specific mole fraction of this material is also 1.48 eV. The QD material is $GaIn_{1-x}As_x$ with different mole fractions. The value of the bandgap of the QD material is [14]
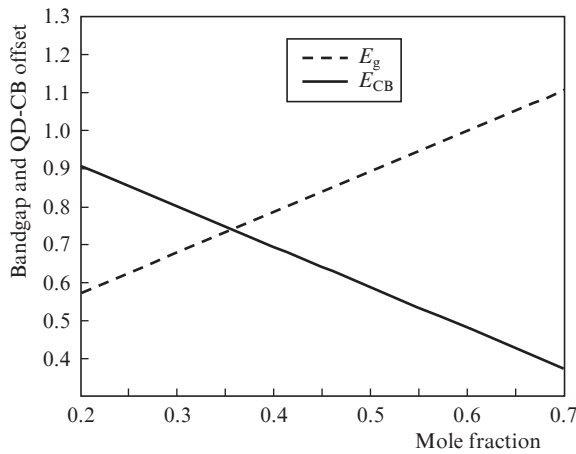
Figure 7. Bandgap and QD-CB offset vs. mole fraction x for GaInAs/GaAsSb/AlAs.
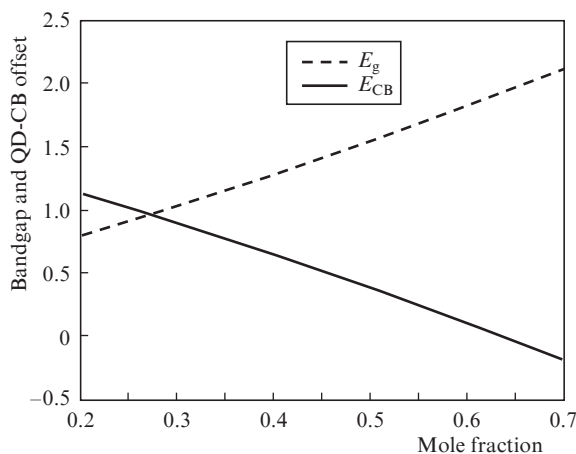
$$E_g = 0.36 + 1.064x. \tag{8}$$

The dependence of the bandgap and the QD-CB offset on the mole fraction is shown in Fig. 7.

Table 2 shows that the CB offset decreases with increasing x; in addition, with decreasing CB offset and increasing QD width, the efficiency decreases. As a result, the maximum efficiency is obtained for larger values of the CB offset and small QD width.

Table 2. Efficiency at different QD parameters for GaInAs/GaAsSb/AlAs.

Mole fraction	CB offset/eV	QD width/nm	Barrier width/nm	Efficiency (%)
0.35	0.75	3.4	2.5	51.92
0.4	0.7	3.9	2.5	52.30
0.5	0.59	4.2	2.5	50.60
0.6	0.49	4.3	2.5	47.87
0.7	0.38	4.5	2.5	44.54

In AlInAs/AlGaAs/AlAs, $Al_xGa_{1-x}As$ with the mole fraction $x = 0.4$ is used as the barrier material. The value of the bandgap of the material is [14]

Figure 8. Bandgap and QD-CB offset vs. mole fraction x for AlInAs/AlGaAs/AlAs.

$$E_g = 1.424 + 1.247x, \tag{9}$$

i.e., $E_g = 1.92$ eV at $x = 0.4$. The QD material in this system is $Al_xIn_{1-x}As$. The bandgap for this material system is

$$E_g = 0.36 + 2.012x + 0.698x^2. \tag{10}$$

The dependence of the bandgap and the QD-CB offset on x is shown in Fig. 8.

It follows from Table 3 that the CB offset decreases with increasing mole fraction. The maximum efficiency is achieved at a CB offset of 0.9 eV and a QD width of 3.6 nm.

Table 3. Efficiency at different QD parameters for AlInAs/AlGaAs/AlAs.

Mole fraction	CB offset/eV	QD width/nm	Barrier width/nm	Efficiency (%)
0.3	0.9	3.6	2.5	55.98
0.35	0.78	3.7	2.5	52.14
0.4	0.65	3.9	2.5	47.58
0.45	0.52	4.2	2.5	43.21
0.5	0.38	4.8	2.5	38.81

4. Conclusions

The relationship between the QD-CB offset and the QD width is important in the design of QD-IBSCs. We have demonstrated that to achieve the maximum efficiency, the QD-CB offset must be increased, whereas the QD width must be decreased and vice versa. Although, an increase in the CB offset increases the efficiency, the maximum efficiency is attained at the QD-CB offset when the energy transitions are located optimally with respect to the optimal width of QDs. Finally, the relationship between the QD-CB offset and the QD width is important in the optimal design of the barrier material and the QD material.

References

1. Marti A., Cuadra L., Luque A. *Proc. Conf. Sobre Dispositivos Electrónicos 1999* (Madrid, 1999) pp 363–366.
2. Green M.A. *Mater. Sci. Eng.*, **74**, 118 (2000).
3. Marti A., Cuadra L., Luque A. *Proc. 28 IEEE Photovoltaics Specialists Conf.* (New York: IEEE, 2000) pp 940–943.
4. Shao Q., Balandin A. *Appl. Phys. Lett.*, **91**, 163503 (2007).
5. Luque A., Marti A. *Phys. Rev. Lett.*, **78** (26), 5014 (1997).
6. Luque A., Marti A. *Prog. Photovoltaics Res. Appl.*, **9** (2), 73 (2001).
7. Marti A. et al. *IEEE Trans. Electron. Devices*, **48**, 2394 (2001).
8. Lopez N., Marti A., Luque A. *J. Sol. Energy Eng.*, **129** (2), 319 (2007).
9. Levy M.Y., Honsberg C., Marti A., Luque A. *Proc. 31 IEEE Photovoltaic Specialists Conf.* (New Jersey: IEEE, 2005) pp 90–93.
10. Jiang Chu Wei, Green M.A. *J. Appl. Phys.*, **99**, 114902 (2006).
11. Lazarenkova O., Balandin A. *J. Appl. Phys.*, **89**, 5509 (2001).
12. Aguinaldo R. *Master Sci. Thes.* (Rochester: Rochester Institute of Technology, 2008).
13. Jenks S., Gilmore R. *J. Renewable Sustainable Energy*, **2**, 013111 (2010).
14. Vurgaftman I. *J. Appl. Phys.*, **89**, 5815 (2001).